Structure analysis and characterization of the cytochrome c-554 from thermophilic green sulfur photosynthetic bacterium Chlorobaculum tepidum

ARTICLE *in* PHOTOSYNTHESIS RESEARCH · SEPTEMBER 2013

Impact Factor: 3.5 · DOI: 10.1007/s11120-013-9922-2 · Source: PubMed

6 AUTHORS, INCLUDING:

Masaki Unno
Ibaraki University
40 PUBLICATIONS **966** CITATIONS
SEE PROFILE

Yukihiro Kimura
Kobe University
37 PUBLICATIONS **631** CITATIONS
SEE PROFILE

Hirozo Oh-Oka
Osaka University
67 PUBLICATIONS **1,093** CITATIONS
SEE PROFILE

Photosynth Res (2013) 118:249–258
DOI 10.1007/s11120-013-9922-2

REGULAR PAPER

Structure analysis and characterization of the cytochrome *c*-554 from thermophilic green sulfur photosynthetic bacterium *Chlorobaculum tepidum*

Long-Jiang Yu · Masaki Unno · Yukihiro Kimura · Kasumi Yanagimoto · Hirozo Oh-oka · Zheng-Yu Wang-Otomo

Received: 11 June 2013 / Accepted: 3 September 2013 / Published online: 20 September 2013

Abstract The cytochrome (Cyt) *c*-554 in thermophilic green photosynthetic bacterium *Chlorobaculum tepidum* serves as an intermediate electron carrier, transferring electrons to the membrane-bound Cyt c_z from various enzymes involved in the oxidations of sulfide, thiosulfate, and sulfite compounds. Spectroscopically, this protein exhibits an asymmetric α-absorption band for the reduced form and particularly large paramagnetic ^{1}H NMR shifts for the heme methyl groups with an unusual shift pattern in the oxidized form. The crystal structure of the Cyt *c*-554 has been determined at high resolution. The overall fold consists of four α-helices and is characterized by a remarkably long and flexible loop between the α3 and α4 helices. The axial ligand methionine has *S*-chirality at the sulfur atom with its $C^{\varepsilon}H_3$ group pointing toward the heme pyrrole ring I. This configuration corresponds to an orientation of the lone-pair orbital of the sulfur atom directed at the pyrrole ring II and explains the lowest-field ^{1}H NMR shift arising from the 18^1 heme methyl protons. Differing from most other class I Cyts *c*, no hydrogen bond was formed between the methionine sulfur atom and polypeptide chain. Lack of this hydrogen bond may account for the observed large paramagnetic ^{1}H NMR shifts of the heme methyl protons. The surface-exposed heme pyrrole ring II edge is in a relatively hydrophobic environment surrounded by several electronically neutral residues. This portion is considered as an electron transfer gateway. The structure of the Cyt *c*-554 is compared with those of other Cyts *c*, and possible interactions of this protein with its electron transport partners are discussed.

Keywords Green sulfur bacteria · Electron transfer · Cytochrome *c* · Axial ligands

Abbreviations

Cba	*Chlorobaculum*
Chl	*Chlorobium*
CD	Circular dichroism
COSY	Correlation spectroscopy
HMQC	Heteronuclear multiple-quantum coherence
MALDI-TOF	Matrix-assisted laser desorption/ionization time-of-flight
MCD	Magnetic circular dichroism
NOESY	Nuclear Overhauser effect spectroscopy
RC	Reaction center

Long-Jiang Yu and Masaki Unno have contributed equally to this study.

Electronic supplementary material The online version of this article (doi:10.1007/s11120-013-9922-2) contains supplementary material, which is available to authorized users.

L.-J. Yu · K. Yanagimoto · Z.-Y. Wang-Otomo (✉)
Faculty of Science, Ibaraki University, Bunkyo 2-1-1, Mito 310-8512, Japan
e-mail: wang@ml.ibaraki.ac.jp

M. Unno
Frontier Research Center for Applied Atomic Science, Ibaraki University, 162-1 Shirakata, Tokai, Naka, Ibaraki 319-1106, Japan

M. Unno
Graduate School of Science and Engineering, Ibaraki University, 4-12-1, Nakanarusawa, Hitachi 316-8511, Japan

Y. Kimura
Organization of Advanced Science and Technology, Kobe University, Nada, Kobe 657-8501, Japan

H. Oh-oka
Department of Biological Sciences, Graduate School of Science, Osaka University, Toyonaka, Osaka 560-0043, Japan

RR	Resonance Raman
Tch	*Thermochromatium*
TOMES	Thiosulfate oxidizing multi-enzyme system

Introduction

In green sulfur bacteria, anoxygenic photosynthesis is carried out using reduced sulfur compounds such as sulfide, elemental sulfur, and thiosulfate as the electron sources. Several oxidizing pathways of the sulfur compounds have been confirmed, and a number of the electron transport proteins have been isolated and characterized (Brune 1995; Sakurai et al. 2010). The final electron carrier to the special pair of bacteriochlorophyll *a* dimer (P840) in the reaction center (RC) is a *c*-type RC-associated cytochrome (Cyt), Cyt c_z (*pscC* gene product) (Oh-oka et al. 1998; Azai et al. 2010). There are two pathways proposed for electron transfer to the Cyt c_z in the well-studied *Chlorobaculum* (*Cba.*) *tepidum*: one is through a soluble mono-heme Cyt *c*-554, and another is through a membrane-bound menaquinol:Cyt *c* oxidoreductase (Tsukatani et al. 2008). The former is considered to be involved in both thiosulfate and sulfide oxidations, while the latter is proposed to gain electrons only from sulfide oxidation. Recently, we have determined the crystal structure of the functional domain of Cyt c_z from *Cba. tepidum* (Hirano et al. 2010). Although its overall structure is highly similar to those of class I Cyts *c* (Moore and Pettigrew 1990), several intriguing features have been observed for its heme environment. For most cases, the imidazole ring plane of the axial His in Cyts *c* is orientated approximately along a line through the heme *meso*-carbons C5 and C15, this plane in Cyt c_z is, however, rotated about 75° clockwise (close to the line through C10 and C20 *meso*-carbons). A water molecule was found in the pocket formed by the CXXCH motif and heme tetrapyrrole ring, which could affect the redox potential. A strong hydrogen bond is formed between the imidazole NH of axial His and the backbone carbonyl of a Thr residue instead of the highly conserved Pro in other Cyts *c*. A hydrophobic patch around the heme pyrrole ring II was proposed as possible binding site of the Cyt c_z to its electron transfer partners.

In this study, we present the crystal structure and characterization of the Cyt *c*-554 from *Cba. tepidum*. This protein has been demonstrated to transfer electrons to the Cyt c_z (Itoh et al. 2002) and to serve as an electron acceptor from a variety of enzymes involved in the sulfide and thiosulfate oxidations, such as flavocytochrome *c* (Kusai and Yamanaka 1973; Davidson et al. 1986), flavoprotein (SoxF) (Ogawa et al. 2010), and the thiosulfate-oxidizing multi-enzyme system (TOMES) complexes (Ogawa et al. 2008; Sakurai et al. 2010). The Cyt *c*-554 exhibits an asymmetric α-absorption band and has a comparatively low redox potential ($E_{m,7} = +148$ mV) (Oh-oka et al. 1998; Itoh et al. 2002). It shares a high sequence homology with Cyts *c* from other green sulfur bacteria although they show slightly different α-absorption peak positions. One of the homologs is the Cyt *c*-555 from *Chlorobium* (*Chl.*) *thiosulfatophilum* which has a sequence identity of 92 % to the Cyt *c*-554 and has been subjected to intensive structural investigation since 1970s. A preliminary result was reported on the crystal structure of the Cyt *c*-555 at 2.7 Å resolution (Korszun and Salemme 1977). However, refinement of the structure was not completed because the spatial arrangement of two fragments each containing about ten residues remained undetermined, and the electron density for the ligated Met was weak (Senn et al. 1984). Therefore, no information on the structure coordinates of this protein is available in the Protein Data Bank (PDB). The oxidized Cyt *c*-555 is characterized by unusually large paramagnetic NMR shifts for all four methyl groups of the heme ring with a particularly large shift for the ring methyl at position 18^1 (Senn et al. 1984). The origin of these large shifts has not been determined. The solution structure of the reduced Cyt *c*-555 was also analyzed by NMR method. The result showed that secondary structure was somewhat different from that observed in the crystal structure, especially for the second helix that is much longer than that in the crystal structure (Morelle et al. 1995). Due to the high sequence similarity, the *Cba. tepidum* Cyt *c*-554 of this study exhibits almost the same spectroscopic and biochemical properties as those of Cyt *c*-555. The high resolution structure of the Cyt *c*-554 will provide useful information for interpreting these unusual properties in relation with its functional role as an electron carrier and also for understanding the mechanism of interactions between the electron transport proteins.

Materials and methods

Expression and purification of the Cyt *c*-554

The procedure used to construct the *Cba. tepidum* Cyt *c*-554 plasmid was similar to that reported previously (Higuchi et al. 2009). A fragment of 261 base pairs in the *cycA* gene coding for the matured portion of Cyt *c*-554 was inserted into the *Sal* I site of the expression vector pET-12a (Novagen Inc., Madison, WI, USA). For expression, the constructed plasmid was co-transformed with pEC86 plasmid (Arslan et al. 1998) into *Escherichia coli* C41(DE3) (Miroux and Walker 1996). Experimental conditions of the expression and purification were the same as

described previously (Higuchi et al. 2009). Under the optimized conditions, the final yield was approximately 7 mg L^{-1} of *E. coli* medium. The resulting protein has a molecular mass of 9561.9 Da as determined by MALDI-TOF/MS (supplementary Fig. S1), indicating that it comprises 86 amino acids of the matured Cyt *c*-554 and two residues (Ser-Thr) attached at the N-terminus due to the *Sal* I restriction site (supplementary Fig. S2). The samples with ratios of $A_{413}/A_{280} > 5.0$ were used for the characterization and crystallization experiments.

Spectroscopic measurements

Absorption, magnetic circular dichroism (MCD), resonance Raman (RR), and one-dimensional ^{1}H NMR spectra of the Cyt *c*-554 were recorded using the same instruments and under the same conditions as described elsewhere (Higuchi et al. 2009; Hirano et al. 2012). For the oxidized and reduced samples, spectra were measured in the presence of 1 mM of potassium ferricyanide and 1 mM of dithiothreitol, respectively, in 30 mM Tris–HCl buffer (pH 8.5). A freshly prepared Cyt *c*-554 sample was used for the RR measurement of each spectrum to minimize the laser-induced degradation. Five spectra from different samples were averaged. Two-dimensional NMR spectra and relaxation times were collected on a Bruker Avance III 500 MHz spectrometer at 25 °C. A 5-mm TXI triple-resonance inverse probe with *z*-axis field gradient was used. NOESY spectra were acquired with mixing times of 30, 50 and 80 ms, spectral width of 25,000 Hz, 256 points in t_1, 2 K points in t_2, and 32 transients for each t_1 points. COSY spectra were acquired with spectral width of 19,000 Hz, 256 points in t_1, 2 K points in t_2, and 16 transients for each t_1 points. ^{1}H-^{13}C HMQC spectra were acquired with spectral widths of 25,000 Hz for ^{1}H and 30,180 Hz for ^{13}C, 128 points in t_1, 2 K points in t_2, and 64 transients for each t_1 points. The spin–lattice ^{1}H relaxation times T_1 were measured using the inverse-recovery ($180° - t - 90°$) method and were calculated by the same procedure as given previously (Wang et al. 2004).

Crystallization and structure determination

The purified Cyt *c*-554 in an air-oxidized state was concentrated to approximately 30 mg mL^{-1} ($OD_{413} \sim 350$). Crystallization was performed using sitting-drop vapor-diffusion method at 20 °C by mixing 2 μL of protein solution with an equal volume of the reservoir solution containing 3.0 M ammonium sulfate, 30 mM zinc chloride and 10 % isopropanol in 50 mM phosphate buffer (pH 5.0). The crystals of Cyt *c*-554 were transferred into the cryoprotectant solution containing the reservoir solution supplemented with 20 % (v/v) glycerol, and then flash frozen in liquid nitrogen. X-ray diffraction data were collected at BL-17A of Photon Factory, Tsukuba, Japan using an ADSC Quantum 315r CCD detector under the following conditions: 100 K, 150 mm detector distance, 0.5° oscillation range, and 1 s exposure time. The data were processed and scaled using the *HKL2000* program package (Otwinowski and Minor 1997). Structure determination was performed by molecular replacement method using the *Molrep* program (Vagin and Teplyakov 1997). The search model used was the crystal structure of Cyt *c*-551 (chain G in PDB code 2ZON) (Nojiri et al. 2009) from *Achromobacter xylosoxidans* GIFU 1051 with the prosthetic groups and solvent molecules removed. 5 % of reflections were used for the free *R* factor calculation in the structure refinement of Cyt *c*-554. The initial model was subjected to rigid body refinement with the *Refmac5* program (Murshudov et al. 1999) followed by incorporation of the heme group and modification of the model was performed using the *Coot* program (Emsley et al. 2010). Positional and isotropic displacement parameters were refined in the resolution range of 45–1.3 Å. After including the solvent molecules in the model, the translation, screw, and libration parameters were refined, and the final model was refined to $R_{work} = 15.1$ % and $R_{free} = 17.0$ %. Coordinates of the crystal structure of the Cyt *c*-554 have been deposited in PDB under accession code 4J20.

Results

The absorption spectrum of oxidized *Cba. tepidum* Cyt *c*-554 (Fig. 1a, broken curve) is typical of low-spin ferric heme with the Soret band at 412.5 nm. When reduced by dithiothreitol, the Soret band shifted to 418 nm with the appearance of α and β bands at 554 and 523 nm (Fig. 1a, solid curve), respectively. The α band is characterized by an asymmetric shape (Fig. 1a, inset and supplementary Fig. S3), which was also observed from the native Cyt *c*-554 (Itoh et al. 2002). Figure 1b shows the corresponding MCD spectra of oxidized and reduced Cyts *c*-554. Overall spectral shapes and the intensity ratio of Soret to α bands indicate a low-spin state of the heme in both oxidized and reduced species. The shape of the α band in the MCD spectrum of reduced Cyt *c*-554 is essentially the same as that of Cyt c_z which has a symmetric shape for the α band in the absorption spectrum (Higuchi et al. 2009). This means that the asymmetric feature in the absorption spectrum of Cyt *c*-554 was not reflected on the MCD spectrum under the current experimental conditions.

Figure 2 shows the RR spectra of Cyt *c*-554 in oxidized and reduced states obtained with *Q*-band excitation. Most of the RR bands can be ascribed to porphyrin in-plane vibrational modes characteristic for the Cyts *c* with a six-

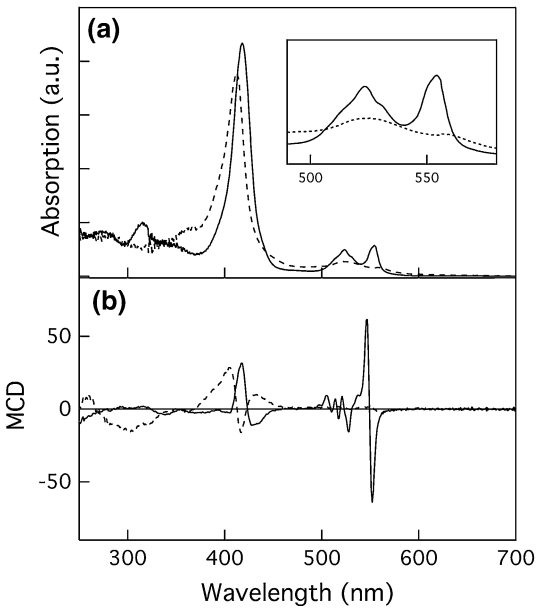

Fig. 1 Absorption (**a**) and MCD (**b**) spectra of the Cyt *c*-554 at oxidized (*broken curves*) and reduced (*solid curves*) states. The samples were dissolved in 30 mM Tris–HCl (pH 8.5) buffers and measured at room temperature. The oxidized state was obtained by addition of potassium ferricyanide at a final concentration of 1 mM, and the reduced state was obtained by addition of dithiothreitol at final concentration of 1 mM

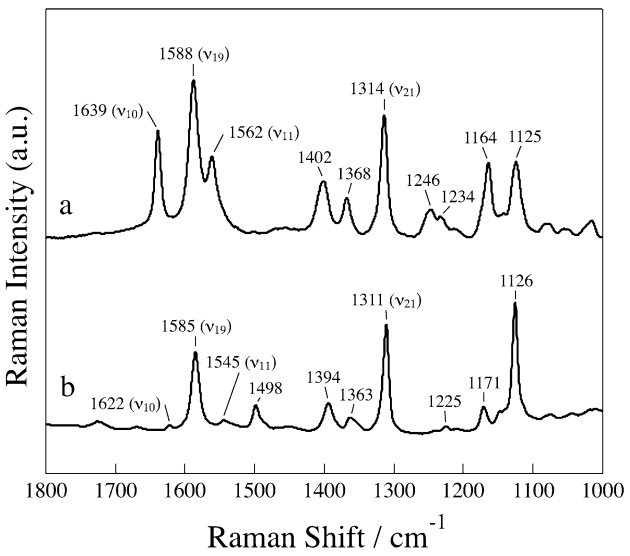

Fig. 2 Resonance Raman spectra of Cyt *c*-554 in 30 mM Tris–HCl buffer (pH 8.5) with 1 mM potassium ferricyanide (*a*) or dithiothreitol (*b*) obtained with 532 nm excitation

coordinated low-spin heme iron (Desbois 1994). In the oxidized spectrum, the 1,639 cm^{-1} (ν_{10}) and 1,562 cm^{-1} (ν_{11}) bands are the RR marker bands for the oxidation of heme irons and are assigned to the asymmetric ν ($C_\alpha C_m$) and ν ($C_\beta C_\beta$) modes, respectively. These bands were red-shifted to 1,622 and 1,545 cm^{-1} in the reduced state with decreasing band intensities. The ν_{11} band in the reduced Cyt *c*-554 indicates a His/Met heme ligation (Desbois 1994) and is comparable with those of other ferrous Cyts *c* (Lewis et al. 1985; Desbois 1994). In contrast, the intensive RR bands at 1,588 cm^{-1} (ν_{19}) and 1,314 (ν_{21}) cm^{-1} in oxidized Cyt *c*-554 were red-shifted to 1,585 and 1,311 cm^{-1}, respectively, upon reduction with little changes in the peak position and intensity. The ν_{19} band for the asymmetric ν ($C_\alpha C_m$) mode is sensitive to the spin state of the heme iron, and the ν_{21} band was assigned to the C_mH bending mode of the heme porphyrin ring (Hu et al. 1993). The ν_{19} band of Cyt *c*-554 was insensitive to the redox change, indicating that the spin state was not altered by reduction under the present condition. In addition, the distance between the imidazole $N^{\varepsilon 2}$ atom of His20 and heme iron deduced from the ν_{19} band frequency was estimated to be 2.0 Å (Spiro et al. 1979) in good agreement with the result obtained from the crystal structure (see below). The ν_{21} mode is sensitive to the conformational change near the heme-binding Cys16 (Shelnutt et al. 1981). Its frequency for the Cyt *c*-554 was similar to those of other ferrous Cyts *c* (Lewis et al. 1985) and was little affected by the redox change, suggesting a similar conformation at the cysteine covalent linkage sites. Beside these marker bands, an intensive peak at 748 cm^{-1} was observed in the low frequency region (supplementary Fig. S4).

Figure 3 shows the temperature-dependence of ^1H NMR spectra of the oxidized Cyt *c*-554 in low and high field regions. Four sharp singlet resonances in the low field are characteristic of heme ring methyl groups and exhibit a pattern similar to that of the Cyt *c*-555 from *Chl. thiosulfatophilum* (Senn et al. 1984). These resonances for Cyt *c*-555 were assigned to the 18^1, 12^1, 7^1, and 2^1 heme methyl protons in order from low to high field (Senn et al. 1984). This assignment was confirmed for the Cyt *c*-554 of this study by NOESY and COSY spectra (data not shown). The large paramagnetic shifts and the shift pattern are different from those of most other class I Cyts *c* and indicate a more extensive spin delocalization of the unpaired electron of the ferric iron in the heme plane and a more symmetrical spin-density distribution (Wüthrich 1976). The highest field resonance at approximately −2.2 ppm was assigned to the $C^\varepsilon H_3$ group of the axial Met residue. While the ^1H chemical shift of 18^1 methyl group decreased slightly with increasing temperature (Curie behavior), many signals shifted markedly to the lower field upon increasing temperature (anti-Curie behavior). Because the configuration of the Met ligand sulfur has been determined by this study to have a *S*-chirality and the $C^\varepsilon H_3$ group points toward pyrrole ring I (see below), the chemical shift pattern of the heme methyl protons is similar to that of the Cyt c_5 from *Pseudomonas mendocina* (Senn and Wüthrich 1983) and can be qualitatively explained in the

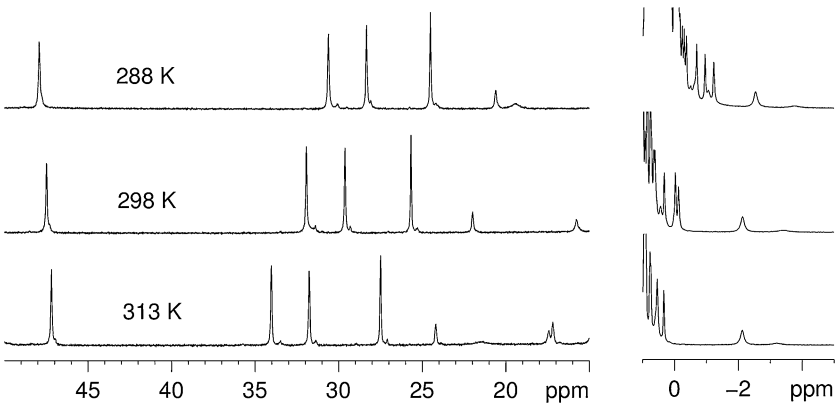

Fig. 3 Extreme low and high field regions of the ^{1}H NMR spectra for the oxidized Cyt *c*-554 at various temperatures. The sample of 1.2 mM was dissolved in 0.1 M sodium phosphate buffer pD 7.0, D_2O/H_2O 90:10 solution

same way as that for the Cyt c_5 although the order of 12^1 and 7^1 is reversed. The ^{13}C chemical shifts of the 12^1, 7^1, and 2^1 heme methyl carbons were determined to be −47.0, −32.6, and −34.5 ppm, respectively, from the HMQC spectra, whereas the signal of 18^1 methyl group was not clearly detected under the experimental condition of this study. ^{1}H relaxation times T_1 were obtained for the heme methyl protons: 51.1 ± 0.3 ms (18^1), 61.2 ± 1.3 ms (12^1), 62.2 ± 0.4 ms (7^1), and 73.2 ± 0.7 ms (2^1). These values are in the same range as those from other heme proteins (McLachlan et al. 1988; Shao et al. 1995; Benini et al. 1998; Gorst et al. 1998; Wei et al. 1998).

Crystals of the air-oxidized Cyt *c*-554 appeared after several months (typically 4–5 months) of crystallization using ammonium sulfate as a precipitant and Zn^{2+} as an additive. Although other divalent metal ions, such as Cu^{2+} and Mg^{2+}, also yielded crystals, Zn^{2+} was found to give the crystals with the highest resolution among these ions. The crystals belong to space group *C*2 with unit cell parameters $a = 94.8$ Å, $b = 33.8$ Å, $c = 47.3$ Å, and $\beta = 107.8°$. Statistics for the data collection and refinement are given in Table 1. The Matthews coefficient was calculated to be 3.69 Å^3 Da^{-1} with two molecules in an asymmetric unit (Fig. 4a), and the solvent content was 33.3 %. The two molecules superpose with a root-mean-square distance of 0.51 Å for 84 C^α atoms. The Cyt *c*-554 consists of four α-helices: α1(5-20), α2(33-40), α3(44-53), and α4(73-85) (Fig. 4b, supplementary Fig. S2). Slightly different conformations between the two molecules are found in the N-terminal region and in the loop from Gly23 to Ala27 between the α1 and α2 helices. The α1 helix is bent around Cys16 and Ala17 with the first segment corresponding to the N-terminal helix of Cyt *c*-555 from *Chl. thiosulfatophilum* as determined by solution NMR (Morelle et al. 1995) and preliminary X-ray crystallography (Korszun and Salemme 1977). Heme-binding motif CATCH is located at the end of α1 helix. The most striking feature is the presence of an extended flexible region of 19 residues between the α3 and α4 helices (Fig. 4b), which is longer than those in most other Cyts *c*. The axial ligand Met62 is located in the middle of the loop. Inter-iron distances are 35.4 Å between the heme groups in chain A and chain B, and 19.3 Å between the heme groups in chain A and chain B* (a symmetry-related molecule to chain B), respectively.

In the crystal structure of *Cba. tepidum* Cyt *c*-554, the heme group covalently binds to the polypeptide chain through thioether linkages of two cysteine residues, Cys16 and Cys19. The axial Met62 has *S*-chirality at the iron-bound sulfur atom with its lone-pair electrons directed at pyrrole ring II (Fig. 5a). The distance between the sulfur

Table 1 Data collection and refinement statistics

Diffraction data	
Space group	*C*2
Cell dimensions (Å)	$a = 94.8$, $b = 33.8$, $c = 47.3$, $\beta = 107.8°$
Wavelength (Å)	1.0
Resolution (Å)	1.3
Unique reflections	35,513
Redundancy	6.4 (4.9)
R_{merge} (%)	6.7 (17.9)
I/σ (I)	51.4 (8.0)
Completeness (%)	98.8 (96.1)
Refinement	
Resolution (Å)	45-1.3
R_{work} (%)	15.2
R_{free} (%)	17.0
No. of protein atoms	1,553
No. of heme atoms	91
No. of solvent atoms	219
Average B-factor (Å^2)	18.26
r.m.s. deviations	
Bonds (Å)	0.031
Angles (°)	2.69
Ramachandran plot (%)	97.65/1.18/1.18

Values in parentheses represent the highest resolution shell

In the crystal structure of *Cba. tepidum* Cyt *c*-554, the heme group covalently binds to the polypeptide chain through thioether linkages of two cysteine residues, Cys16 and Cys19. The axial Met62 has *S*-chirality at the iron-bound sulfur atom with its lone-pair electrons directed at pyrrole ring II (Fig. 5a). The distance between the sulfur

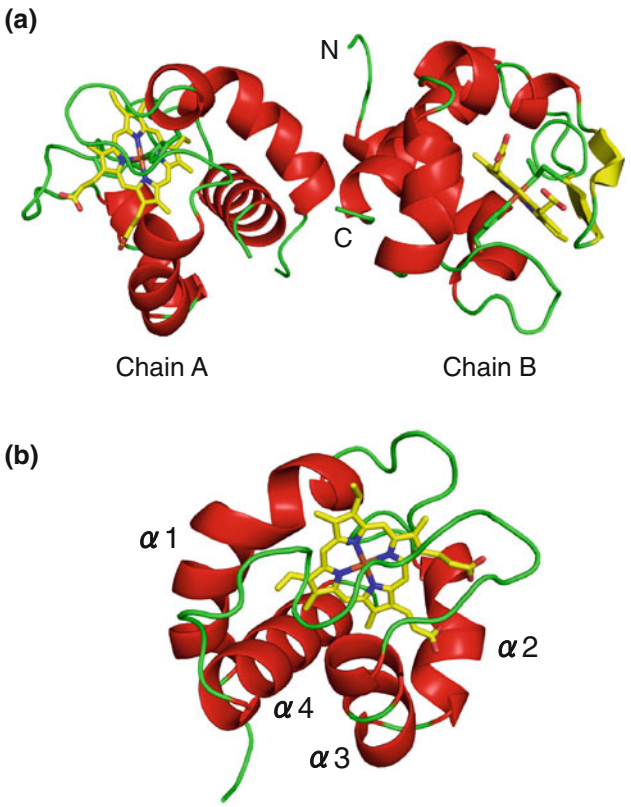

Fig. 4 Crystal structure of the *Cba. tepidum* Cyt *c*-554. **a** Two Cyt *c*-554 molecules in the asymmetric unit. The positions of N- and C-termini are indicated in chain B. **b** Close-up view of the heme group and the extended loop in chain A

atom and heme iron is 2.33 Å (2.34 Å, the value in parenthesis denotes that for chain B hereinafter). The C^{ε} points toward pyrrole ring I forming a dihedral angle of 68.6° (66.8°) between the C^{ε}–S bond and a line connecting the heme iron and the *meso*-carbon C5. This configuration closely resembles those in Cyts c_5 of *Pseudomonas mendocina* (Senn and Wüthrich 1983) and *Azotobacter vinelandii* (Carter et al. 1985). The latter has a dihedral angle of 71.4°. The spatial arrangement of axial Met62 in Cyt *c*-554 accounts for the lowest field resonance of 18^1 heme methyl protons as observed in the NMR spectrum (Fig. 3). Unlike what occurs in most other class I Cyts *c*, the sulfur atom does not form hydrogen bond with the polypeptide chain. Another ligand His20 coordinates to the heme iron with the imidazole ring orientated perpendicularly to the heme plane along a line through the *meso*-carbons C5 and C15 (Fig. 5b). The distance between the $N^{\varepsilon 2}$ atom and heme iron is 2.02 Å (2.01 Å). The $N^{\delta 1}$ atom of His20 forms a hydrogen bond with the carbonyl oxygen of a nearby residue (Pro28) as observed for most other Cyts *c*. The heme propionates form hydrogen bond networks with neighboring polypeptide and water molecules. In chain A, the propionate-13 forms hydrogen bonds with the side chains of Arg39 and Tyr55 and one water molecule, while the network involved with propionate-17 consists of the side chains of Arg39, Gln42, and Lys50 with two water molecules. A similar pattern was observed in chain B except that Lys50 was not involved in the hydrogen bonding.

Most of the surface area of the Cyt *c*-554 is covered with charged and polar residues (Fig. 6), and the heme group is largely embedded in the hydrophobic interior. The only parts that are solvent accessible in heme are the pyrrole ring II and propionate groups. The protein surface around the pyrrole ring II edge consists of several electronically neutral residues and forms an open gate with Ala14, Thr18, and Met25 located on one side and Met61, Pro63, and Gly67 on the other. This portion is relatively hydrophobic

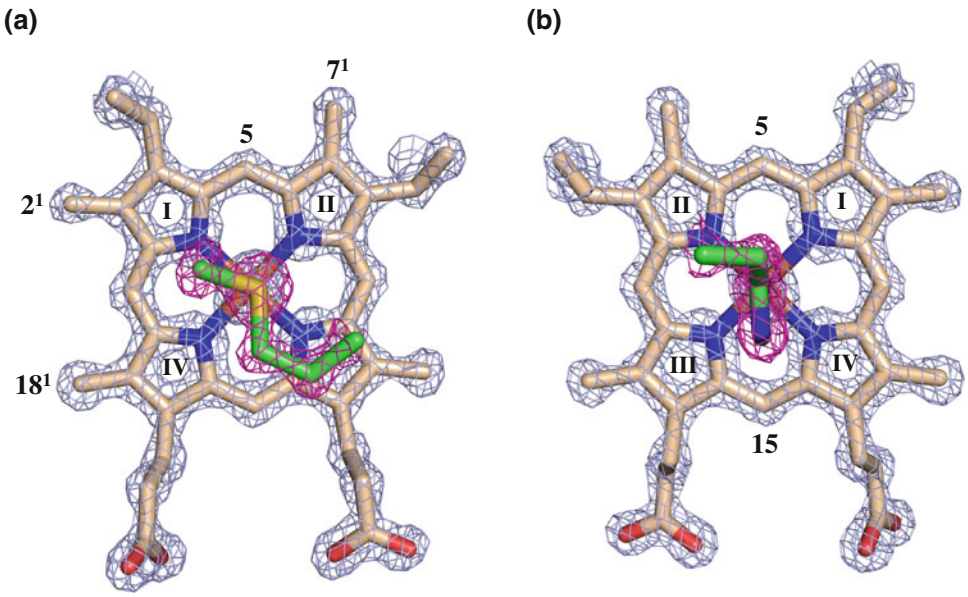

Fig. 5 Electron density maps and the assigned structures of heme group and side chains of the coordinating residues. The final $2F_o - F_c$ density maps are shown as mesh contoured at 2.0 σ level, heme and side chains are shown as stick models. The *Roman numbers* denote the pyrrole rings. **a** Conformation and orientation of the axial Met62 side chain with respective to the heme plane (*front*). **b** Conformation and orientation of the imidazole ring of the axial His20 residue with respective to the heme plane (*back*)

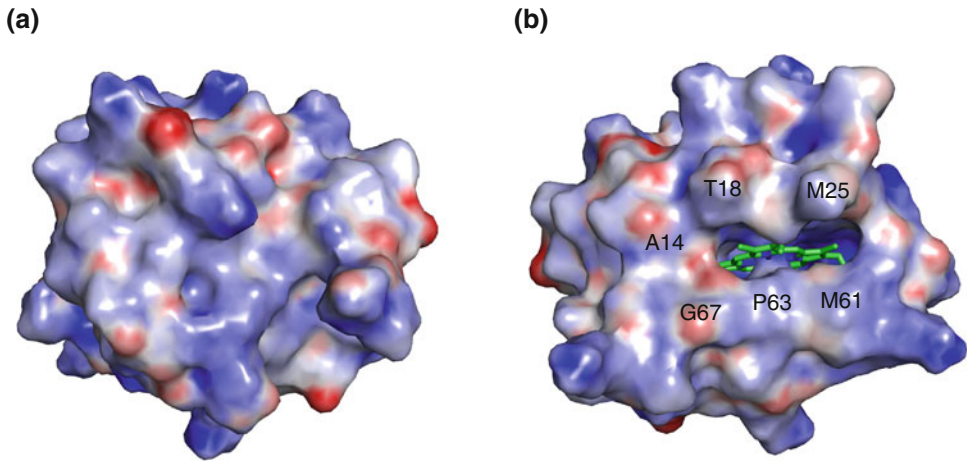

Fig. 6 **a** Electrostatic property of the surface of Cyt *c*-554. The distribution is colored according to the electrostatic potential from $-20k_BT$ (*red*) to $+20k_BT$ (*blue*). **b** The opposite side of **a** showing the surface-exposed heme group (*green*) and the positions of surrounding residues

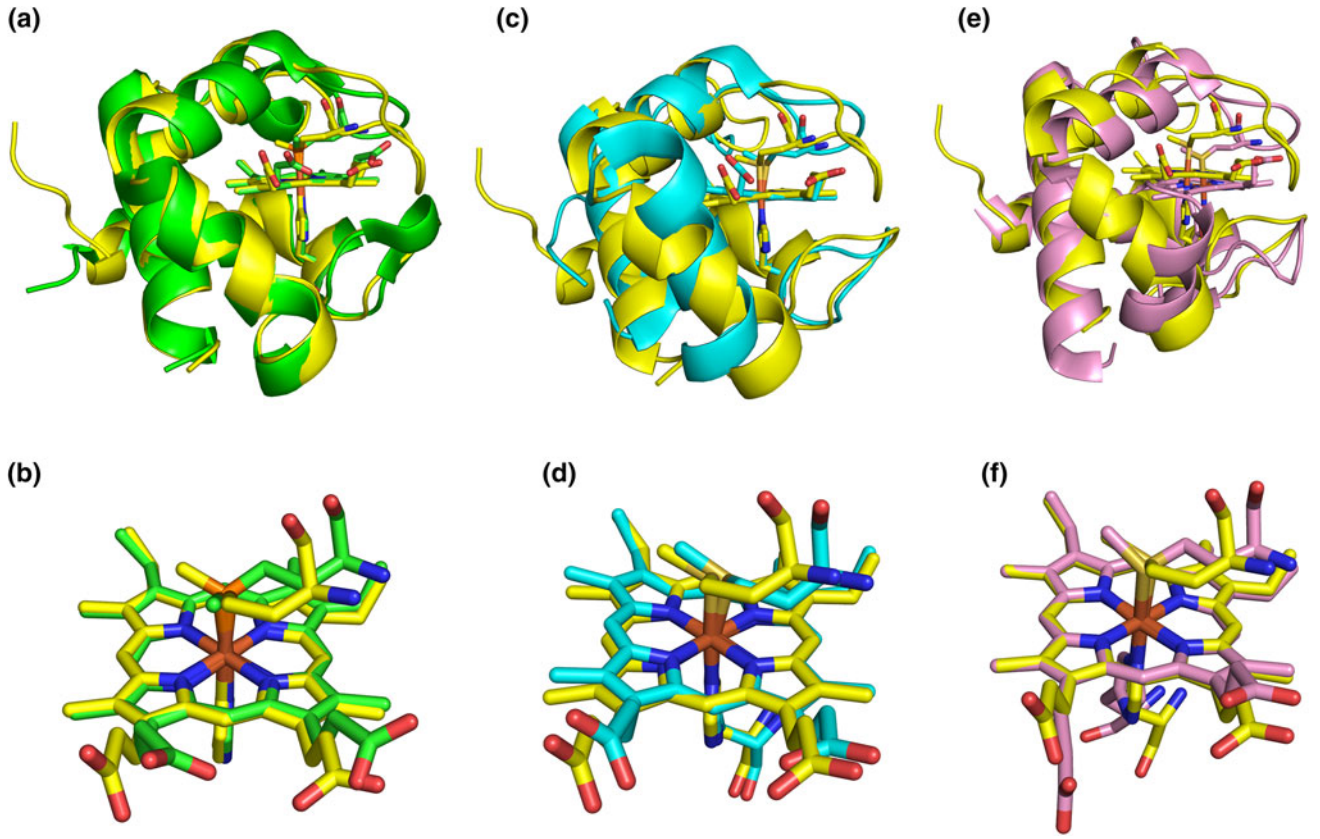

Fig. 7 Structure comparison of the *Cba. tepidum* Cyt *c*-554 (*yellow*) with Cyt *c*-551 from *Achromobacter xylosoxidans* (*green*; PDB code 2ZON), Cyt c_5 from *Azotobacter vinelandii* (*cyan*; PDB code 1CC5), and Cyt c_6 from *Phormidium laminosum* (*pink*; PDB code 2V08). **a** Superposition of the polypeptide chains of Cyt *c*-554 and Cyt *c*-551. **b** Close-up view of the heme groups and the axial ligands in **a**. **c** Superposition of the polypeptide chains of Cyt *c*-554 and Cyt c_5. **d** Close-up view of the heme groups and the axial ligands in **c**. **e** Superposition of the polypeptide chains of Cyt *c*-554 and Cyt c_6. **f** Superposition of the heme groups of Cyt *c*-554 and Cyt c_6

and is considered as an electron transport pathway as reported for other Cyts *c*. Four water molecules form a network cluster around this region in chain A, whereas only one water molecule is located close to the heme *meso*-carbon C10 in chain B.

The overall structure of the *Cba. tepidum* Cyt *c*-554 reveals high similarities to those of Cyt *c*-551 from *Achromobacter xylosoxidans* (Nojiri et al. 2009), Cyt c_5 from *Azotobacter vinelandii* (Carter et al. 1985) and Cyts c_6 from a variety of species with the *Z*-scores of 15.1, 11.3, and 7.8–10.1, respectively (Holm and Rosenström 2010) (Fig. 7, supplementary Fig. S2). The crystal structure of Cyt c_6 from cyanobacterium *Phormidium laminosum* (*Z*-score: 9.9) (Worrall et al. 2007) was chosen for

comparison. The major difference in protein fold between the Cyt *c*-554 and other proteins is found in the flexible region between α3 and α4 helices, where the Cyt *c*-554 has a much longer loop. The axial methionine in Cyt c_6 has an *R*-chirality, while all other proteins have *S*-chirality. Despite the high similarity in structures between Cyt *c*-554 and Cyt *c*-551, the axial methionine in Cyt *c*-551 shows a different orientation with the C^{ε} almost pointing toward the heme *meso*-carbon C15. The dihedral angle is 175.2° between the C^{ε}–S bond and a line connecting the heme iron and the *meso*-carbon C5. In addition, the side chain of methionine in Cyt *c*-551 has a *cis* orientation along the C^{γ}–S bond in contrast to those in Cyt *c*-554, Cyt c_5, and Cyt c_6.

Discussion

Cba. tepidum Cyt *c*-554 expressed in *E. coli* shows absorption spectra resembling those of the native one purified from the same bacterium (Oh-oka et al. 1998; Itoh et al. 2002) typically in the region of α and β bands for the reduced form (Fig. 1). Because these bands result from the coupling between electronic and vibrational states for two mixed (0, 0) transitions, the position and shape of the α band are extremely sensitive to a small perturbation of the heme geometry or a change in the polarity of the heme environment (Moore and Pettigrew 1990). The resemblance of its asymmetric feature ensures that the Cyt *c*-554 used in this study has the same structure as the native one. It is of interest to note that the spectral shape of the α band is very similar to that of Cyt c_6 (also known as algal or cyanobacterial Cyt *c*-553) (Yamanaka and Okunuki 1968), which functions as an electron donor to the RC of photosystem I in higher photosynthetic organisms and also has a structure similar to that of the Cyt *c*-554.

The present RR analysis demonstrated that the characteristic bands of Cyt *c*-554 appeared at similar positions with those of other six-coordinated low-spin Cyts *c*. However, a distinct difference was observed in the low frequency region below 1,000 cm^{-1} (supplementary Fig. S4), where the 748 cm^{-1} band assigned to a pyrrole breathing mode (ν_{15}) was unusually enhanced in the reduced state of Cyt *c*-554. Similar enhancement was observed in the spectra of reduced flavocytochrome *c* from purple sulfur bacterium *Thermochromatium* (*Tch.*) *tepidum* but not in those of Cyt c_z from *Cba. tepidum* and Cyt *c* from horse heart, under similar conditions. It was suggested that the very strong RR band for the ν_{15} mode as well as the red-shift of Soret band is associated with the symmetry lowering of the heme plane due to a distortion of the porphyrin macrocycle (Hu et al. 1993). Actually, the Soret peak of reduced Cyts *c* appeared in the order of Cyt *c*-554 (418 nm) > flavocytochrome *c* (416 nm) (Hirano et al. 2012) > Cyt c_z (415 nm) (Higuchi et al. 2009) >Cyt *c* (414 nm). In addition, the relative intensity of the α band toward the Soret band is inversely proportional to the 748 cm^{-1} band intensity. Although the relationship between the unusual ν_{15} band and the electronic structure of reduced Cyt *c*-554 is unclear, it is implied that some conformational distortion of the heme macrocycle by a small perturbation in the heme environment is responsible not only for the enhanced RR band at 748 cm^{-1} but also the unusual absorption properties, including the red-shift of the Soret band and asymmetry of the α band in the reduced Cyt *c*-554.

The ^{1}H NMR paramagnetic shift pattern of the heme methyl groups in oxidized Cyt *c*-554 is same as that reported previously for its homolog Cyt *c*-555 from *Chl. thiosulfatophilum* (Senn et al. 1984), and the assignment has been confirmed in this study. The spread and order of these shifts are significantly different from those of most other Cyts *c* (Senn and Wüthrich 1985; Shokhirev and Walker 1998). They are characterized by unusually large paramagnetic shifts for all heme methyl groups with a particularly large shift for the 18^1 protons. The average of the four methyl shifts for Cyt *c*-554 is 33.7 ppm at 298 K, which is much greater than those of most other heme proteins (below 25 ppm) (Shokhirev and Walker 1998). Although the origin of these large paramagnetic shifts has not been determined, it was strongly suggested that the unusual electronic structure is due to a particular coordination geometry of the axial methionine (Senn et al. 1984). Based on the crystal structure of Cyt *c*-554, we propose that one of the factors may be the lack of a hydrogen bond formed between the sulfur atom of axial Met62 and the polypeptide chain. For most class I Cyts *c*, the lone-pair electrons of the sulfur atom are involved in hydrogen bonding with a tyrosine O^{η} or Asn N^{δ}. Lack of this hydrogen bond could strengthen interactions of the lone-pair electrons with the d_{xz} and d_{yz} orbitals of the iron, resulting in a more extensive delocalization of the unpaired electron of the low-spin ferric iron in the heme plane. A similar case has been observed for Cyt c_z, which also lacks such hydrogen bond and the average of the four methyl shifts is 31.1 ppm (Higuchi et al. 2009; Hirano et al. 2010). On the other hand, the assignment of the lowest-field resonance (18^1) in Cyt *c*-554 can also be interpreted in terms of its crystal structure. The axial Met62 shows an *S*-stereochemistry at the chiral sulfur ligand and the C^{ε} points toward pyrrole ring I (Fig. 5a). As a consequence, the sp^3 lone-pair orbital of the sulfur atom is orientated along a line through the nitrogen atoms of the pyrrole rings II and IV. This configuration is essentially identical to those of the axial methionines in Cyts c_5 of *Pseudomonas mendocina* (Senn and Wüthrich 1983) and *Azotobacter vinelandii* (Carter et al. 1985). The former shows lowest field

resonance for the heme 18^1 protons. The difference in the order of chemical shifts for the 7^1 and 12^1 methyl protons between Cyt *c*-554 and Cyt c_5 may be attributed to subtle differences in the coordination geometry (Fig. 7) as the spin-density distributions are relatively more symmetrical for these proteins.

The physiological role of the Cyt *c*-554 in *Cba. tepidum* has been shown as an intermediate electron carrier, transferring electrons to the membrane-bound Cyt c_z from various enzymes involved in oxidations of sulfide, thiosulfate, and sulfite compounds. The rate constant of electron transfer from Cyt *c*-554 to Cyt c_z was estimated to be 1.7×10^7 M^{-1} s^{-1} (Itoh et al. 2002). Although the Cyt *c*-554 and the functional domain of Cyt c_z show low sequence homology (13 % identity) and relatively low overall structural similarity (*Z*-score 3.4), both of them belong to the same group of class I Cyts *c* and the local geometry for electron transfer seems to be conserved. The crystal structure of the functional domain of Cyt c_z reveals that the region of the surface-exposed heme pyrrole ring II is a possible binding site to another electron transfer partner (Hirano et al. 2010), a similar feature to that of Cyt *c*-554. Attempts to co-crystallize the Cyt c_z and Cyt *c*-554 have not been successful. On the other hand, it has been demonstrated that the Cyt *c*-554 can accept electrons from a monomeric SoxF involved in the sulfide oxidation in *Cba. tepidum* (Ogawa et al. 2010). The SoxF shows a high sequence similarity to the FAD-binding subunit (FccB, 49 % identity) of a flavocytochrome *c* from the purple sulfur bacterium *Thermochromatium* (*Tch.*) *tepidum* (Hirano et al. 2012). Using the known structure of *Tch. tepidum* FccB as a template, a structural model for the SoxF can be generated by the homology modeling tool, SWISS-MODEL (Arnold et al. 2006). An interacting model for the SoxF/Cyt *c*-554 complex could be constructed (supplementary Fig. S5) based on the protein–protein docking analysis (Lyskov and Gray 2008), where the SoxF interacts with Cyt *c*-554 in a similar way to the pair of SoxF and diheme subunits in the flavocytochrome *c* and the distance between the two prosthetic groups is 20.6 Å from the heme Fe and O4 of the isoalloxazine ring. The Cyt *c*-555 of *Chl. thiosulfatophilum*, a mesophilic homologue of the *Cba. tepidum* Cyt *c*-554, has been shown to function as an electron acceptor from flavocytochrome *c* (Kusai and Yamanaka 1973) and to form electrostatically stabilized complexes with the flavocytochromes *c* not only from the same bacterium but also from its counterpart in purple sulfur bacterium *Chromatium vinosum* (Davidson et al. 1986). The binding sites for the Cyt *c*-555 in both complexes seem to be located on the diheme-containing subunits of flavocytochromes *c*. In view of the significant catalytic and structural similarities between the mesophilic and thermophilic electron transfer pairs, we have examined the possibility of a heterogeneous complex formation between the thermophilic protein partners. Preliminary evidence has been obtained from size-exclusion chromatography, showing that the *Cba. tepidum* Cyt *c*-554 and *Tch. tepidum* flavocytochrome *c* appear to form such a complex. Further investigation of the interaction between the two proteins and co-crystallization of the complex are in progress. The information along with the results of this study should provide structural insights into the mechanism of a sequential electron transfer along a series of electron carriers and the geometry of prosthetic groups in the electron flow pathway.

Acknowledgments We thank M. Higuchi for technical assistance. This work was supported by Grants-in-aid for Scientific Research on Priority Areas "Structures of Biological Macromolecular Assemblies" (to Z.-Y.W-O.) and Grants-in-aid for Scientific Research (C) (No. 24570183 to H. O.), from the Ministry of Education, Culture, Sports, Science and Technology of Japan, and partially supported by The Kurata Memorial Hitachi Science and Technology Foundation. The X-ray experiments were performed under the approval of the Photon Factory Program Advisory Committee (Proposal No. 2009G525 and 2011G514), and we thank the beamline staff for their help in data collection.

References

Arnold K, Bordoli L, Kopp J, Schwede T (2006) The SWISS-MODEL workspace: a web-based environment for protein structure homology modelling. Bioinformatics 22:195–201

Arslan E, Schulz H, Zufferey R, Künzler P, Thöny-Meyer L (1998) Overproduction of the *Bradyrhizobium japonicum c*-type cytochrome subunits of the cbb_3 oxidase in *Escherichia coli*. Biochem Biophys Res Commun 251:744–747

Azai C, Tsukatani Y, Itoh S, Oh-oka H (2010) *C*-type cytochromes in the photosynthetic electron transfer pathways in green sulfur bacteria and heliobacteria. Photosynth Res 104:189–199

Benini S, Borsari M, Ciurli S, Dikiy A, Lamborghini M (1998) Modulation of *Bacillus pasteurii* cytochrome c_{553} reduction potential by structural and solution parameters. J Biol Inorg Chem 3:371–382

Brune DC (1995) Sulfur compounds as photosynthetic electron donors. In: Blankenship RE, Madigan MT, Bauer CE (eds) Anoxyenic photosynthetic bacteria. Kluwer Academic Publishers, The Netherlands, pp 847–870

Carter DC, Melis KA, O'Donnell SE, Burgess BK, Furey WF Jr, Wang B-C, Stout CD (1985) Crystal structure of *Azotobacter* cytochrome c_5 at 2.5 Å resolution. J Mol Biol 184:279–295

Davidson MW, Meyer TE, Cusanovich MA, Knaff DB (1986) Complex formation between *Chlorobium limicola* f. *thiosulfatophilum c*-type cytochromes. Biochim Biophys Acta 850:396–401

Desbois A (1994) Resonance Raman spectroscopy of c-type cytochromes. Biochimie 76:693–707

Emsley P, Lohkamp B, Scott WG, Cowtan K (2010) Features and development of Coot. Acta Crystallogr D D66:486–501

Gorst CM, Wilks A, Yeh DC, de Montellano PRO, La Mar GN (1998) Solution ^{1}H NMR investigation of the molecular and electronic structure of the active site of substrate-bound human heme oxygenase: the nature of the distal hydrogen bond donor to bound ligands. J Am Chem Soc 120:8875–8884

Higuchi M, Hirano Y, Kimura Y, Oh-oka H, Miki K, Wang Z-Y (2009) Overexpression, characterization, and crystallization of

the functional domain of cytochrome c_z from *Chlorobium tepidum*. Photosynth Res 102:77–84

Hirano Y, Higuchi M, Oh-oka H, Miki K, Wang Z-Y (2010) Crystal structure of the electron carrier domain of the reaction center cytochrome c_z subunit from green photosynthetic bacterial *Chlorobium tepidum*. J Mol Biol 397:1175–1187

Hirano Y, Kimura Y, Suzuki H, Miki K, Wang Z-Y (2012) Structure analysis and comparative characterization of the cytochrome *c*' and flavocytochrome *c* from thermophilic purple photosynthetic bacterium *Thermochromatium tepidum*. Biochemistry 51:6556–6567

Holm L, Rosenström P (2010) Dali server: conservation mapping in 3D. Nucleic Acids Res 38:W545–W549

Hu S, Morris IK, Singh JP, Smith KM, Spiro TG (1993) Complete assignment of cytochrome c resonance Raman spectra via enzymic reconstitution with isotopically labeled hemes. J Am Chem Soc 115:12446–12458

Itoh M, Seo D, Sakurai H, Sétif P (2002) Kinetics of electron transfer between soluble cytochrome *c*-554 and purified reaction center complex from the green sulfur bacterium *Chlorobium tepidum*. Photosynth Res 71:125–135

Korszun ZR, Salemme FR (1977) Structure of cytochrome c_{555} of *Chlorobium thiosulfatophilum*: primitive low-potential cytochrome *c*. Proc Natl Acad Sci USA 74:5244–5247

Kusai A, Yamanaka T (1973) Cytochrome *c* (553, *Chlorobium thiosulfatophilum*) is a sulfide-cytochrome *c* reductase. FEBS Lett 34:235–237

Lewis MA, Timkovich R, Cotton TM (1985) A comparative study of the resonance Raman spectra of bacterial cytochromes. Arch Biochem Biophys 236:515–525

Lyskov S, Gray JJ (2008) The RosettaDock server for local protein–protein docking. Nucleic Acids Res 36:W233–W238

McLachlan SJ, La Mar GN, Lee K-B (1988) One- and two-dimensional nuclear Overhauser effect studies of the electronic/molecular structure of the heme cavity of ferricytochrome b_5. Biochim Biophys Acta 957:430–445

Miroux B, Walker JE (1996) Over-production of proteins in *Escherichia coli*: mutant hosts that allow synthesis of some membrane proteins and globular proteins at high levels. J Mol Biol 260:289–298

Moore GR, Pettigrew GW (1990) Cytochromes c: evolutionary structural and physicochemical aspects. Springer, Berlin

Morelle N, Simorre J-P, Caffrey M, Meyer T, Cusanovich M, Marion D (1995) ^{1}H and ^{13}C NMR assignment and secondary structure of *Chlorobium limicola* f. *thiosulfatophilum* ferrocytochrome c_{555}. FEBS Lett 365:172–178

Murshudov GN, Levedev A, Vagin AA, Wilson KS, Dodson EJ (1999) Efficient anisotropic refinement of macromolecular structure using FFT. Acta Crystallogr D D55:247–255

Nojiri M, Koteishi H, Nakagami T, Kobayashi K, Inoue T, Yamaguchi K, Suzuki S (2009) Structural basis of inter-protein electron transfer for nitrite reduction in denitrification. Nature 462:117–120

Ogawa T, Furusawa T, Nomura R, Seo D, Hosoya-Matsuda N, Sakurai H, Inoue K (2008) SoxAX binding protein, a novel component of the thiosulfate-oxidizing multienzyme system in the green sulfur bacterium *Chlorobium tepidum*. J Bacteriol 190:6097–6110

Ogawa T, Furusawa T, Shiga M, Seo D, Sakurai H, Inoue K (2010) Biochemical studies of a *soxF*-encoded monomeric flavoprotein purified from the green sulfur bacterium *Chlorobaculum tepidum* that stimulates in vitro thiosulfate oxidation. Biosci Biotechnol Biochem 74:771–780

Oh-oka H, Iwaki M, Itoh S (1998) Membrane -bound cytochrome c_z couples quinol oxidoreductase to the P840 reaction center complex in isolated membranes of the green sulfur bacterium *Chlorobium tepidum*. Biochemistry 37:12293–12300

Otwinowski Z, Minor W (1997) Processing of X-ray diffraction data collected in oscillation mode. In: Charles W, Carter J, Robert MS (eds) Methods in enzymology macromolecular crystallography part A, vol 276. Academic Press, New York, pp 307–326

Sakurai H, Ogawa T, Shiga M, Inoue K (2010) Inorganic sulfur oxidizing system in green sulfur bacteria. Photosynth Res 104:163–176

Senn H, Wüthrich K (1983) A new spatial structure for the axial methionine observed in cytochrome c_5 from *Pseudomonas mendocina*. Biochim Biophys Acta 747:16–25

Senn H, Wüthrich K (1985) Amino acid sequence, haem-iron co-ordination geometry and functional properties of mitochondrial and bacterial c-type cytochromes. Quart Rev Biophys 18:111–134

Senn H, Cusanovich MA, Wüthrich K (1984) ^{1}H NMR assignments for the heme group and electronic structure in *Chlorobium thiosulfatophilum* cytochrome *c*-555. Biochim Biophys Acta 785:46–53

Shao W, Sun H, Yao Y, Tang W (1995) ^{1}H NMR studies of the imidazole complex of cytochrome *c*: resonance assignment and structural characterization of the heme cavity. Inorg Chem 34:680–687

Shelnutt JA, Rousseau DL, Dethmers JK, Margoliash E (1981) Protein influences on porphyrin structure in cytochrome *c*. Biochemistry 20:6485–6497

Shokhirev NV, Walker FA (1998) The effect of axial ligand plane orientation on the contact and pseudocontact shifts of low-spin ferriheme proteins. J Biol Inorg Chem 3:581–594

Spiro TG, Stong JD, Stein P (1979) Porphyrin core expansion and doming in heme proteins. New evidence from resonance Raman spectra of six-coordinate high-spin ion(III) hemes. J Am Chem Soc 101:2648–2655

Tsukatani Y, Azai C, Kondo T, Itoh S, Oh-oka H (2008) Parallel electron donation pathways to cytochrome c_z in the type I homodimeric photosynthetic reaction center complex of *Chlorobium tepidum*. Biochim Biophys Acta 1777(9):1211–1217. doi:10.1016/j.bbabio.2008.05.002

Vagin A, Teplyakov A (1997) MOLREP: an automated program for molecular replacement. J Appl Cryst 30:1022–1025

Wang Z-Y, Kadota T, Kobayashi M, Kasuya A, Nozawa T (2004) NMR relaxation study of the bacteriochlorophyll *c* in solutions. J Phys Chem B 108:15422–15428

Wei X, Ming L-J, Cannons AC, Solomonson LP (1998) ^{1}H and ^{13}C NMR studies of a truncated heme domain from *Chlorella vulgaris* nitrate reductase: signal assignment of the heme moiety. Biochim Biophys Acta 1382:129–136

Worrall JAR, Schlarb-Ridley BG, Reda T, Marcaida MJ, Moorlen RJ, Wastl J, Hirst J, Bendall DS, Luisi BF, Howe CJ (2007) Modulation of heme redox potential in the cytochrome c_6 family. J Am Chem Soc 129:9468–9475

Wüthrich K (1976) NMR in biological research: peptides and proteins. North-Holland, Amsterdam

Yamanaka T, Okunuki K (1968) Comparison of *Chlorobium thiosulphatophilum* cytochrome *c*-555 with *c*-type cytochromes derived from algae and nonsulphur purple bacteria. J Biochem 63:341–346